



1 **Identification of hydrological model parameters variation using**  
2 **ensemble Kalman filter**

3

4 Chao Deng<sup>1,2</sup>, Pan Liu<sup>1,2,\*</sup>, Shenglian Guo<sup>1,2</sup>, Zejun Li<sup>1,2</sup>, Dingbao Wang<sup>3</sup>

5

6 <sup>1</sup>State Key Laboratory of Water Resources and Hydropower Engineering Science, Wuhan University,  
7 Wuhan 430072, China

8 <sup>2</sup>Hubei Provincial Collaborative Innovation Center for Water Resources Security, Wuhan 430072,  
9 China

10 <sup>3</sup>Department of Civil, Environmental & Construction Engineering, University of Central Florida,  
11 Orlando 32816, USA

12

13 \*Corresponding author: P. Liu, State Key Laboratory of Water Resources and Hydropower  
14 Engineering Science, Wuhan University, Wuhan 430072, China

15 Email: liupan@whu.edu.cn

16 Tel: +86-27-68775788; Fax: +86-27-68773568



17 **Abstract:** Hydrological model parameters play an important role in the ability of model prediction. In  
18 a stationary context, parameters of hydrological models are treated as constants; however, model  
19 parameters may vary with time under climate change and human activities. The technique of ensemble  
20 Kalman filter (EnKF) is proposed to identify the temporal variation of parameters for a two-parameter  
21 monthly water balance model (TWBM) by assimilating the runoff observations. Through a synthetic  
22 experiment, the proposed method is evaluated with time-invariant (i.e., constant) parameters and  
23 different types of parameter variations, including trend, abrupt change, and periodicity. Various levels of  
24 observation uncertainty are designed to examine the performance of the EnKF. The results show that the  
25 EnKF can successfully capture the temporal variations of the model parameters. The application to the  
26 Wudinghe basin shows that the water storage capacity ( $SC$ ) of the TWBM model has an apparent  
27 increasing trend during the period from 1958 to 2000. The identified temporal variation of  $SC$  is  
28 explained by land use and land cover changes due to soil and water conservation measures. Whereas,  
29 the application to the Tongtianhe basin shows that the estimated  $SC$  has no significant variation during  
30 the simulation period of 1982-2013, corresponding to the relatively stationary catchment characteristics.  
31 The evapotranspiration parameter ( $C$ ) has temporal variations while no obvious change patterns exist.  
32 The proposed method provides an effective tool for quantifying the temporal variations of the model  
33 parameters, thereby improving the accuracy and reliability of model simulations and forecasts.

34



- 35 **Keywords:** model parameter identification, temporal variation of parameter, catchment characteristics,  
36 ensemble Kalman filter



## 37 **1 Introduction**

38 Hydrological model parameters are critically important for accurate simulation of runoff. Parameters of  
39 conceptual hydrological models can be considered as a simplified representation of the physical  
40 characteristics in hydrologic processes. Therefore, parameter values are closely related to the catchment  
41 conditions, such as climate change, afforestation and urbanization (Peel et al., 2011). In hydrological  
42 modeling, parameters are usually assumed to be stationary, i.e., the calibrated parameters are constants  
43 during the calibration period, and have extrapolative ability outside the range of the observations used  
44 for parameter estimation (Merz et al., 2011). However, the calibration period may contain different  
45 climatic conditions and hydrological regimes compared to the simulation period (Merz et al., 2011;  
46 Zhang et al., 2011; Westra et al., 2014; Patil and Stieglitz, 2015). The model parameters may change  
47 responding to the variations in climatic conditions and catchment properties. For example, land use and  
48 land cover changes contribute to temporal changes of model parameters (Andréassian et al., 2003;  
49 Brown et al., 2005; Merz et al., 2011). As a result, the estimated parameters usually depend on the  
50 calibration period (Merz et al., 2011; Coron et al., 2012; Seiller et al., 2012; Westra et al., 2014).  
51 Therefore, assuming time-invariant model parameters may be unrealistic, especially for catchments with  
52 time-varying climate conditions and/or catchment characteristics.

53

54 The time-variant hydrological model parameters has been reported in a few recent publications (Merz et



55 al., 2011; Brigode et al., 2013; Jeremiah et al., 2014; Thirel et al., 2014; Westra et al., 2014; Patil and  
56 Stieglitz, 2015). For example, Ye et al. (1997) and Paik et al. (2005) mentioned the seasonal variations  
57 of hydrological model parameters. Merz et al. (2011) analyzed the temporal changes of model  
58 parameters, which were calibrated respectively by using six consecutive 5-year periods between 1976  
59 and 2006 for 273 catchments in Austria. Recently, Westra et al. (2014) proposed a strategy to cope with  
60 nonstationarity of hydrological model parameters, which were represented as a function of a  
61 time-varying covariate set before using an optimization algorithm for calibration. Previous studies  
62 provided two main methods to estimate the time-variant model parameters: (1) Parameters are estimated  
63 for each consecutive subsets divided from the historical record using an optimization algorithm (Merz et  
64 al., 2011; Thirel et al., 2015); (2) A functional form of the selected time-variant model parameters is  
65 constructed and, the parameters for the function are estimated using an optimization algorithm based on  
66 the entire historical record (Jeremiah et al., 2014; Westra et al., 2014).

67

68 The data assimilation (DA) actually provides another method to identify the potential temporal  
69 variations of model parameters by updating them in real-time when observations are available (Liu and  
70 Gupta, 2007; Xie and Zhang, 2013). The DA method has been widely applied in hydrology for soil  
71 moisture estimation (Han et al., 2012; Kumar et al., 2012) and flood forecasting (Liu et al., 2013; Abaza  
72 et al., 2014). It has also been successfully used to estimate model parameters (Moradkhani et al., 2005;



73 Panzeri et al., 2013; Vrugt et al., 2013; Xie and Zhang, 2013; Shi et al., 2014; Xie et al., 2014). For  
74 example, Vrugt et al. (2013) proposed two types of Particle-DREAM method to track the evolving  
75 target distribution of HyMOD parameters, while the true parameters were assumed to be constant. Xie  
76 and Zhang (2013) used a partitioned forecast-update scheme based on the EnKF to retrieve optimal  
77 parameters in a distributed hydrological model. Although the DA method has been used to estimate  
78 model parameters, these studies are focused on the estimation of constant parameters. Little attention  
79 has been paid to the identification of time-variant model parameters and the interpretation of their  
80 temporal variations based on the climate conditions and/or catchment characteristics.

81

82 The aim of this study is to assess the capability of the DA method (i.e., the EnKF) to identify the  
83 temporal variations of the model parameters for a monthly water balance model. Thus, a synthetic  
84 experiment, including four scenarios with different parameter variations and one scenario with  
85 time-invariant parameters, is designed for parameter estimation at different uncertainty levels.  
86 Furthermore, two case studies are implemented to estimate the model parameter series and to interpret  
87 the parameter variations in response to the changes in catchment characteristics, i.e., land use and land  
88 cover. The remainder of this paper is organized as follows. Section 2 presents a brief review of the  
89 monthly water balance model and the EnKF method. Following the methodology, Section 3 describes  
90 the synthetic experiment and the application to two case studies. Results and discussion are presented in



91 Section 4, followed by conclusions in Section 5.

92

## 93 **2 Methodology**

### 94 **2.1 Monthly water balance model**

95 The two-parameter monthly water balance model (TWBM), developed by Xiong and Guo (1999), has  
96 been widely applied for monthly runoff simulation and forecast (Guo et al., 2002; Guo et al., 2005;  
97 Xiong and Guo, 2012; Li et al., 2013; Zhang et al., 2013; Xiong et al., 2014). The inputs of the model  
98 include monthly areal precipitation and potential evapotranspiration. The actual monthly  
99 evapotranspiration is calculated as follows:

$$100 \quad E_i = C \times EP_i \times \tanh(P_i / EP_i) \quad (1)$$

101 where  $E_i$  represents the actual monthly evapotranspiration;  $EP_i$  and  $P_i$  are the monthly potential  
102 evapotranspiration and precipitation, respectively;  $C$  is the first model parameter; and  $i$  is the time  
103 step.

104

105 The monthly runoff is dependent on the soil water content and is calculated by the following equation:

$$106 \quad Q_i = S_i \times \tanh(S_i / SC) \quad (2)$$

107 where  $Q_i$  is the monthly runoff; and  $S_i$  is the soil water content. As the second model parameter,  
108  $SC$  represents the water storage capacity of the catchment in millimeter. The available water for



109 runoff at the  $i$ th month is computed by  $S_{i-1} + P_i - E_i$ . Then, the monthly runoff is calculated as:

$$110 \quad Q_i = (S_{i-1} + P_i - E_i) \times \tanh\left[\frac{(S_{i-1} + P_i - E_i)}{SC}\right] \quad (3)$$

111

112 Finally, the soil water content at the end of each time step is updated based on the water conservation

113 law:

$$114 \quad S_i = S_{i-1} + P_i - E_i - Q_i \quad (4)$$

115

## 116 **2.2 Ensemble Kalman filter**

117 EnKF is a typical sequential data assimilation technique based on the Monte Carlo method and

118 produces an ensemble of state simulations to update the state variables and model parameters,

119 conditioned on a series of observations (Moradkhani et al., 2005; Shi et al., 2014). It is applicable to a

120 variety of nonlinear problems (Evensen, 2003; Weerts and El Serafy, 2006) and has been widely

121 applied to hydrological models (Abaza et al., 2014; DeChant and Moradkhani, 2014; Delijani et al.,

122 2014; Samuel et al., 2014; Tamura et al., 2014; Xue and Zhang, 2014; Deng et al., 2015). Furthermore,

123 the EnKF has been successfully used in time-invariant parameter estimations for hydrological models

124 (Moradkhani et al., 2005; Wang et al., 2009; Xie and Zhang, 2010; Xie and Zhang, 2013).

125

126 In this paper, the EnKF is applied to simultaneously estimate state variables and parameters (**Table 1**)





127 in the TWBM model. The augmented state vector includes both states and model parameters (Wang et  
 128 al., 2009), i.e.,  $Z = \begin{pmatrix} \theta \\ x \end{pmatrix}$ , where  $\theta$  includes the evapotranspiration parameter  $C$  and the catchment  
 129 water storage capacity  $SC$ , and  $x$  is the soil water content  $S$ . The model forecast is conducted for  
 130 each ensemble member as follows:

$$131 \begin{pmatrix} \theta_{i+1|i}^k \\ x_{i+1|i}^k \end{pmatrix} = \begin{pmatrix} \theta_{i|i}^k \\ f(x_{i|i}^k, \theta_{i+1|i}^k, u_{i+1}) \end{pmatrix} + \begin{pmatrix} \delta_i^k \\ \varepsilon_i^k \end{pmatrix}, \text{ where } \delta_i^k \sim N(0, U_i), \varepsilon_i^k \sim N(0, G_i) \quad (5)$$

132 where  $\theta_{i+1|i}^k$  is the  $k$ th ensemble member forecast of model parameters at time  $i+1$ ;  $\theta_{i|i}^k$  is the  $k$ th  
 133 updated ensemble member of model parameters at time  $i$ ;  $x_{i+1|i}^k$  is the  $k$ th ensemble member forecast  
 134 of model state at time  $i+1$ ;  $x_{i|i}^k$  is the  $k$ th updated ensemble member of model state at time  $i$ ;  $f$  is  
 135 the forecasting model operator, i.e. the TWBM model;  $u_{i+1}$  is the forcing data for the hydrological  
 136 model, including precipitation and potential evapotranspiration;  $\varepsilon_i^k$  and  $\delta_i^k$  are the independent  
 137 white noise for the forecasting model, followed a Gaussian distribution with zero mean and specified  
 138 covariance  $G_i$  and  $U_i$ , respectively. Note that the parameters in Eq. (5) are propagated by adding  
 139 random disturbances to the parameter member between time steps (Wang et al., 2009).

140  
 141 The observation ensemble member can be written as:

$$142 y_{i+1}^k = h(x_{i+1|i}^k, \theta_{i+1|i}^k) + \xi_{i+1}^k, \xi_{i+1}^k \sim N(0, W_{i+1}) \quad (6)$$

143 where  $y_{i+1}^k$  is the  $k$ th ensemble member of the model simulated runoff at time  $i+1$ ;  $h$  is the



144 observation operator which represents the relationship between the observation and the state variables;

145  $\xi_{i+1}^k$  is the noise term which follows a Gaussian distribution with zero mean and specified covariance

146  $W_{i+1}$ .

147

148 Based on the available state and observation equations, the model parameters and state are updated

149 according to the following equation:

$$150 \quad Z_{i+1|i+1}^k = Z_{i+1|i}^k + K_{i+1} \left( y_{i+1}^k - h \left( Z_{i|i}^k \right) \right) \quad (7)$$

151 where  $Z$  is the augmented state vector that includes both state and parameters;  $y_{i+1}^k$  is the  $k$ th

152 observation ensemble member generated by adding the observation error  $\xi_{i+1}^k$  to the observed runoff:

$$153 \quad y_{i+1}^k = y_{i+1} + \xi_{i+1}^k \quad (8)$$

154  $K_{i+1}$  is the Kalman gain matrix that represents the weight between the forecasts and observations. It

155 can be calculated as (Moradkhani et al., 2005):

$$156 \quad K_{i+1} = \sum_{i+1|i}^{zy} \left( \sum_{i+1|i}^{yy} + W_{i+1} \right)^{-1} \quad (9)$$

157 where  $\sum_{i+1|i}^{zy}$  is the cross covariance of the forecasted state and parameters;  $\sum_{i+1|i}^{yy}$  is the error

158 covariance of the forecasted output. The error covariance matrix is calculated based on the forecasted

159 ensemble members:

$$160 \quad \sum_{i+1|i} = \frac{1}{N-1} Z_{i+1|i} Z_{i+1|i}^T \quad (10)$$

161 where  $Z_{i+1|i} = \left( z_{i+1|i}^1 - z_{i+1|i}^m, \dots, z_{i+1|i}^N - z_{i+1|i}^m \right)$  and  $z_{i+1|i}^m$  is the ensemble mean of the forecasted members,



162 and  $N$  is the ensemble size.

163

164 Since the parameters are limited within a range, the constrained EnKF (Wang et al., 2009) is used in this

165 study. The ensemble size, uncertainties in input and output have significant impacts on the assimilation

166 performance of the EnKF, and they are specified following the previous studies (Moradkhani et al.,

167 2005; Wang et al., 2009; Xie and Zhang, 2010; Nie et al., 2011; Lü et al., 2013; Samuel et al., 2014).

168 Generally, larger ensemble size causes the propagation of more accurate error information but leads to

169 computational burden (Moradkhani et al., 2005; Xie and Zhang, 2010). In this study, there are only

170 three variables including two model parameters and one state variable in the assimilation process. To

171 satisfy the estimation accuracy and the computational efficiency, the ensemble size is set to 1000 for the

172 synthetic experiment and the two case studies. In the present study, the uncertainties, including state

173 variable and parameter errors ( $\varepsilon$  and  $\delta$  in Eq. (5), respectively), and runoff observation error ( $\xi$  in Eq.

174 (6)), are assumed to follow a Gaussian distribution with zero mean and specified covariance. Note that

175 the model parameter errors should vary relying on the hydrological model used and the study basin

176 (Clark et al., 2008). Larger standard deviation can generate greater perturbations to model parameters,

177 and it can improve the coverage of updated parameters but also may cause fluctuations in the estimates.

178 In this study, the parameter errors are determined empirically, i.e., the standard deviation of  $C$  is set to

179 0.01 for all the cases, while that of  $SC$  is set to 5.0, 1.0 and 0.5 in the synthetic experiment, Wudinghe



180 basin and Tongtianhe basin, respectively. The standard deviations of both model state and observation  
181 errors are assumed to be proportional to the magnitude of true values (Wang et al., 2009; Lü et al.,  
182 2013). The proportional factors of model state are set to 0.05 for all the cases. Different proportional  
183 factors of runoff observation and precipitation (**Table 3**) are evaluated to examine the capability of the  
184 EnKF in the synthetic experiment; whereas, the proportional factors of runoff observation are set to 0.1  
185 and zero precipitation errors are assumed in the two case studies. It should be noted that the variable  
186 variance multiplier can be used to perturb the observations (Leisenring and Moradkhani, 2012; Yan et  
187 al., 2015).

188

### 189 **2.3 Evaluation index**

190 Two evaluation criteria, including the Nash-Sutcliffe efficiency (*NSE*) (Nash and Sutcliffe, 1970) and  
191 the volume error (*VE*) are used to evaluate the runoff assimilation results for the synthetic experiment  
192 and the application to real catchments (Deng et al., 2015; Li et al., 2015).

$$193 \quad NSE = 1 - \frac{\sum_{i=1}^n (Q_{sim,i} - Q_{obs,i})^2}{\sum_{i=1}^n (Q_{obs,i} - \bar{Q}_{obs})^2} \quad (11)$$

$$194 \quad VE = \frac{\sum_{i=1}^n Q_{sim,i} - \sum_{i=1}^n Q_{obs,i}}{\sum_{i=1}^n Q_{obs,i}} \quad (12)$$

195 where  $Q_{sim,i}$  and  $Q_{obs,i}$  are the simulated and observed runoff for the  $i$ th month;  $\bar{Q}_{obs}$  is the mean  
196 values of the observed runoff; and  $n$  is the total number of data points. The *NSE* has been widely



197 used to assess the goodness-of-fit for hydrological modeling. A *NSE* value of 1 means a perfect match  
 198 of simulated runoff to the observations. The *VE* is a measure of bias between the simulated and  
 199 observed runoff. For example, *VE* with the value of 0 denotes no bias, and a negative value means an  
 200 underestimation of the total runoff volume.

201

202 The assimilated parameter results are evaluated using the following criteria, including the Pearson  
 203 correlation coefficient (*R*), the root mean square error (*RMSE*) and mean absolute relative error  
 204 (*MARE*):

$$205 \quad R = \frac{\sum_{i=1}^n (\theta_{sim,i} - \bar{\theta}_{sim})(\theta_{obs,i} - \bar{\theta}_{obs})}{\sqrt{\sum_{i=1}^n (\theta_{sim,i} - \bar{\theta}_{sim})^2 (\theta_{obs,i} - \bar{\theta}_{obs})^2}} \quad (13)$$

$$206 \quad RMSE = \sqrt{\frac{1}{n} \sum_{i=1}^n (\theta_{sim,i} - \theta_{obs,i})^2} \quad (14)$$

$$207 \quad MARE = \frac{1}{n} \sum_{i=1}^n \frac{|\theta_{sim,i} - \theta_{obs,i}|}{\theta_{obs,i}} \quad (15)$$

208 where  $\theta_{sim,i}$  and  $\theta_{obs,i}$  are the assimilated and true model parameters for the *i* th month;  $\bar{\theta}_{sim}$  and  
 209  $\bar{\theta}_{obs}$  are the mean of the assimilated and true model parameters, respectively for the *i* th month; *n* is  
 210 the total number of data points.

211

### 212 **3 Data and study area**



### 213 **3.1 Synthetic experiment**

214 A synthetic experiment is designed to evaluate the capability of the assimilation procedure to identify  
215 the temporal variation of model parameters. Five scenarios of different parameter variations are  
216 developed, as shown in **Table 2**. The model parameters in the first four scenarios are time-variant, and  
217 those in the last scenario are constant. Parameter *C*, the evapotranspiration parameter, is considered to  
218 be sinusoidal reflecting potential seasonal variations in hydrological model parameters (Paik et al., 2005;  
219 Ye et al., 1997). An increasing trend is also considered to account for the potential annual or long-term  
220 variability. The change of parameter *SC* is considered to be gradual and abrupt, since the catchment  
221 water storage capacity can be affected by land use and land cover changes, such as afforestation and  
222 dam construction. The parameters in Scenario 5 are treated as constants like the conventional  
223 hydrological modeling. Observations for precipitation and potential evapotranspiration are generated by  
224 adding a Gaussian disturbance to the corresponding data from a real catchment, and runoff is then  
225 produced using the TWBM model. The data set used in this experiment includes a total of 672 months.  
226 The first 24-month period is set for model warm-up to reduce the impact of the initial soil moisture  
227 conditions. The steps toward identifying temporal variation of model parameters are as follows:  
228 (1) Time series of model parameters are generated, including the time-variant parameters and the  
229 constant parameters. Model parameter sets are produced using a sinusoidal function and/or a linear  
230 trend function within the specified ranges shown in **Table 1**. The runoff observations for each scenario



231 are computed from the TWBM model taking monthly potential evapotranspiration and precipitation,  
232 and the parameters as inputs.

233 (2) The initial ensembles of model parameters and state variables are generated using uniform  
234 distributions within the specified ranges in **Table 1**. The ensemble size and the total number of  
235 assimilation time steps are specified.

236 (3) After the initialization of parameters and state variables, the hydrological model parameters and  
237 states are updated by assimilating the runoff observations obtained in Step (1). The additive errors for  
238 generating the ensemble members of model parameters, state variables and runoff observations are  
239 obtained from Gaussian distributions with zero mean and specified variance.

240

241 To evaluate the effect of errors on identifying parameter variation, different levels of observation  
242 uncertainty are considered in the synthetic experiment, as detailed in **Table 3**. The uncertainties from  
243 the observed precipitation and runoff are characterized by adding Gaussian noises where the standard  
244 deviations are assumed to be proportional to the magnitude of the true values, and the corresponding  
245 proportional factors are denoted as  $\gamma_P$  and  $\gamma_Q$ . The proportional factors are set to account for the  
246 practical measurement error (Wang et al., 2009; Xie and Zhang, 2010).

247

## 248 **3.2 Study area**



### 249 **3.2.1 Case 1: Wudinghe basin**

250 The method is applied to the Wudinghe basin (**Fig. 1**), which is a sub-basin of the Yellow River basin  
251 and located in the southern fringe of Maowusu Desert and the northern part of the Loess Plateau in  
252 China with a semiarid climate. It has a drainage area of approximately 30,261 km<sup>2</sup> and a total length of  
253 491 km. The Wudinghe basin has an average slope of 0.2%, and its elevation ranges from 600 to 1800  
254 m above the sea level. The Baijiachuan gauge station, which is the most downstream station of the  
255 Wudinghe basin, drains 98% of the total basin area. The mean annual precipitation over the basin is  
256 401 mm, of which 72.5% occurs in the rainy season from June to September (**Fig. 2**). The mean  
257 annual potential evapotranspiration is 1077 mm, and the mean annual runoff is about 39 mm with a  
258 runoff coefficient of 0.1.

259  
260 The soil erosion is severe in the Wudinghe basin owing to the highly erodible loess and sparse  
261 vegetation. Since the 1960s, the soil and water conservation measures have been undertaken. Lots of  
262 engineering measures including tree and grass plantation, check dam and reservoir construction, and  
263 land terracing were effectively implemented during several decades. The land use changes caused by  
264 the soil and water conservation measures had a significant effect on increasing water storage capacity  
265 (Xu, 2011).

266





### 267 **3.2.2 Case 2: Tongtianhe basin**

268 The Tongtianhe basin (**Fig. 3**) is located in southwestern Qinghai Province in China with a continental  
269 climate. It belongs to the source area of Yangtze River basin with a drainage area of about 140,000 km<sup>2</sup>  
270 and a total main stream length of 1206 km. The elevation of the Tongtianhe basin approximately ranges  
271 from 3500 to 6500 m above the sea level. Zhimenda is the basin outlet. The mean annual precipitation  
272 over the basin is 440 mm, of which 76.9% occurs in the period from June to September (**Fig. 4**). The  
273 mean annual potential evapotranspiration is 796 mm, and the mean annual runoff is about 99 mm with a  
274 runoff coefficient of 0.23. The Tongtianhe basin is barely affected by human activities owing to the  
275 limitation of the topographic condition and the water source protection guidelines conducted by the  
276 government. The Tongtianhe basin is used for comparison on model parameter identification.

277

### 278 **3.2.3 Data**

279 The data sets used in this study include monthly precipitation, potential evapotranspiration and runoff in  
280 Wudinghe basin (from 1956 to 2000) and Tongtianhe basin (from 1980 to 2013). The potential  
281 evapotranspiration is estimated using the Penman-Monteith equation (Allen et al., 1998) based on the  
282 meteorological data from the China Meteorological Data Sharing Service System (<http://cdc.nmic.cn>).  
283 To reduce the impact of the initial conditions, a 2-year data set, i.e., from 1956 to 1957 for Wudinghe  
284 basin and from 1980 to 1981 for Tongtianhe basin, is reserved as the warm-up period.



285

## 286 **4 Results and discussion**

### 287 **4.1 Synthetic experiment**

288 The comparisons of the estimated and true model parameters under different scenarios are presented  
289 in **Fig. 3**, **Fig. 4** and **Fig. 5**. **Tables 4** and **5** show the evaluation statistics for the parameters and runoff  
290 estimations. The assimilated parameter values are obtained from the ensemble mean at each time step.  
291 The estimations of parameter  $C$  and  $SC$  have the similar trends as the true parameter series. The  
292 temporal variations of the estimated  $C$  agree well with the true series, although it has biases on the  
293 peaks of the periodic changes. For  $SC$ , the temporal estimates can capture the different changes in  
294 **Table 2**, especially for the abrupt change where the estimated values respond immediately. Different  
295 uncertainty levels are considered to examine the capability of the EnKF method. The results in **Fig. 3**  
296 show that the estimated  $C$  has more accurate peaks with smaller  $RMSE$  and higher  $R$  values under the  
297 high level uncertainty (**Table 4**); whereas, the  $SC$  estimates in **Fig. 4** have some fluctuations when the  
298 uncertainty level increases. This is due to the reason that the estimated values vary with increasing  
299 uncertainty level in the assimilation process. In the synthetic experiment, the true  $C$  is assumed to be  
300 periodic with higher degree of variation, while the true  $SC$  series have less variation.

301

302 It should be noted that there are time lags between the assimilated and true  $C$ . The observation at the



303 current time step is used to adjust the state variables and parameters in EnKF, and the updates of  
304 parameters depend on the Kalman gain for parameters. A runoff observation at the current time is  
305 determined by states at the current and previous time steps (Pauwels and Lannoy, 2006). The Kalman  
306 gain is dependent on the relative value of observation error to model error. The updated states are  
307 closer to the observation with a higher Kalman gain (Tamura et al., 2014). The synthetic *C* series were  
308 assumed to be periodic where lots of peak values exist; while the variation of *SC* series is less. The  
309 time lag between assimilated and true values exists especially when peak values occur (Clark et al.,  
310 2008; Samuel et al., 2014).

311

312 The results for the scenario of constant parameters are shown in **Fig. 5**, demonstrating that the  
313 estimated parameters can approach their true values after the initial 24 assimilation steps. The grey  
314 areas represent the 95% uncertainty intervals, which reduce quickly and approach to a stable spread.  
315 The performance of the estimated parameters is correlated with the uncertainty level. Higher  
316 precipitation and runoff observation errors correspond to greater *RMSE* values (**Table 4**) of estimated  
317 parameters and uncertainty ranges. The performance of runoff estimations for various parameter  
318 changes under different levels of uncertainty is shown in **Table 5**, suggesting that the EnKF perfectly  
319 matches the observations with NSEs higher than 0.95 and absolute VEs smaller than 0.02. The EnKF  
320 can successfully capture the temporal variations of the true parameters, although the uncertainty levels



321 of the observations can affect its performance on a certain degree. The above results demonstrate that  
322 the EnKF is able to identify the temporal variation of the model parameters by updating the state  
323 variables and parameters based on the runoff observations.

324

## 325 **4.2 Case studies**

326 **Fig. 6** shows the double mass curve between monthly runoff and precipitation for the Wudinghe and  
327 Tongtianhe basins, respectively. The top panel shows the linear relationship between cumulative runoff  
328 and precipitation pre- and post-1972 in the Wudinghe basin, which is similar to the result presented by  
329 Xu (2011) and Li et al. (2014). The results show two straight lines with different slopes for the  
330 relationships between precipitation and runoff, indicating that an abrupt change occurred in 1972,  
331 namely, the runoff generation had been changed from this year due to the soil and water conservation  
332 measures. While the bottom panel demonstrates a single linear relationship fits all the data for the  
333 Tongtianhe basin, suggesting a stable precipitation-runoff relationship during the 1982-2013 period.

334

335 The estimated parameters and the associated 95% uncertainty intervals are shown in **Fig. 7**. The time  
336 series of estimated *SC* shows an apparent increasing trend, with two different trends for pre- and  
337 post-turning point in **Fig. 6(a)**. The temporal variation of the water storage capacity is correlated with  
338 the changes of land use and land cover. Both the trends in **Fig. 7(c)** show an increase of *SC*, because the



339 implementation of the large-scale engineering measures significantly improved the water holding  
340 capacity of the Wudinghe basin, especially for the reservoir and check dam construction. The trend  
341 slopes of the two periods, one is from 1956 to 1971, the other is from 1972 to 2000, are different  
342 because the degree of implementing engineering measures varied during the period of 1958-2000.  
343 Moreover, the increase of the water holding capacity slowed down during the 1980s due to the  
344 sedimentation in reservoirs and check dams after periods of operation (Wang and Fan, 2003). **Fig. 8**  
345 shows the runoff reduction caused by all the soil and water conservation measures, i.e., land terracing,  
346 tree and grass plantation, check dam and reservoir construction. The runoff reduction positively relates  
347 to the water holding capacity, namely the  $SC$  value. The slope for the period of 1958-1971 is higher than  
348 that for the period of 1972-1996, suggesting that the  $SC$  in the former period has higher increasing trend.  
349 The runoff reduction data is available from 1956 to 1996 (Wang and Fan, 2003). On the other hand, the  
350 result of Tongtianhe basin shows that the estimated  $SC$  has no detectable trend since the  $R$  value has  
351 an insignificance level. Moreover, the ranges and standard deviation of the estimated  $SC$  values are  
352 much smaller than those in the Wudinghe basin (**Fig. 7**), suggesting that the estimated  $SC$  has no  
353 obvious temporal variations.

354

355 For parameter  $C$ , the results show that the estimates have no obvious temporal patterns because the  
356 trend line slopes are almost zero and the standard deviations are relatively small for the two basins (**Fig.**



357 **7(a)** and **(b)**). However, the temporal variations exist in the estimated  $C$  values, indicating that this  
358 parameter has different values during the time steps and can be treated as time-variant parameters. The  
359 temporal variations of the estimated  $C$  are related to the variation of monthly actual evaporation, which  
360 is affected by multiple climatic factors, such as air temperature, soil moisture and solar irradiance (Su et  
361 al., 2015). The grey regions represent the 95% uncertainty intervals obtained from the parameter  
362 ensembles. The stable and narrow uncertainty bounds shown in **Fig. 7** indicate that the EnKF can  
363 provide superior performance of parameter estimation. The runoff simulations for both the two basins  
364 have good match with the runoff observations. Specifically, the  $NSE$  and  $VE$  for the Wudinghe basin are  
365 0.93 and 0.07 respectively. While the corresponding index values are 0.99 and 0.04 for the Tongtianhe  
366 basin.

367  
368 In summary, the above results demonstrate that the EnKF can identify the temporal variation of model  
369 parameters well by updating both state variables and parameters based on the runoff observations. The  
370 trends of parameter  $SC$  can be explained by the changes of catchment characteristics (i.e., land use  
371 and land cover) in the Wudinghe basin. However, the estimated  $SC$  for the Tongtianhe basin is  
372 approximately stable with small standard deviation because the basin is located in a water protection  
373 zone and has no significant changes on water storage capacity caused by human activities. The  
374 parameter  $C$  has temporal variations and can be treated as a time-variant parameter for both basins,



375 although the estimates have no obvious temporal patterns. Therefore, the EnKF is capable of identifying  
376 the temporal variations of model parameters.

377

## 378 **5 Conclusions**

379 This study proposes an ensemble Kalman filter (EnKF) to identify the temporal variation of model  
380 parameters in the two-parameter monthly water balance model (TWBM) by assimilating the runoff  
381 observations. A synthetic experiment, which contains four scenarios with different changes of model  
382 parameters and one scenario with constant parameters, is designed to examine the capability of the  
383 proposed approach. Furthermore, three different levels of observation uncertainty are taken to assess  
384 the performance of the EnKF. The main conclusions are drawn as follows: For the time-variant  
385 parameters, the EnKF can provide superior performance even though slight time lags exist when  
386 parameters have periodic variations. The true values of the constant parameters can be approached  
387 quickly after 24 time steps of assimilation process. The temporal variations of the parameters can be  
388 successfully captured under a high level of uncertainty, although the observation uncertainties from  
389 precipitation and runoff have an influence on the performance of the EnKF.

390

391 The EnKF method is applied to the Wudinghe basin in China, aiming to detect the temporal variations  
392 of the model parameters and to provide an explanation for the parameter variation from the perspective



393 of the catchment characteristic changes. Meanwhile, a comparison is implemented to investigate the  
394 variation of model parameters in the Tongtianhe basin, which is barely affected by human activities. The  
395 parameter of water storage capacity ( $SC$ ) for the monthly water balance model shows a significant  
396 increasing trend for the period of 1958-2000 in the Wudinghe basin. The soil and water conservation  
397 measures, including land terracing, tree and grass plantation, check dam and reservoir construction,  
398 have been implemented during 1958 to 2000, resulting in the increase of the water holding capacity of  
399 the basin, which explains the increasing trends of  $SC$ . Moreover, the magnitudes of the engineering  
400 measures in different time periods play an important role in the degree of increasing trend for  $SC$ . In the  
401 Tongtianhe basin, the parameter  $SC$  has no significant trend for the period of 1982-2013, which is  
402 consistent with the relatively stationary catchment characteristics. The evapotranspiration parameter ( $C$ )  
403 has temporal variations and can be treated as time-variant parameter, but no obvious trends exist.

404

405 The method proposed in this paper provides an effective tool for the time-variant model parameters  
406 identification. Future work will be focused on the influence of the correlations between/among model  
407 parameters and performance comparison of multiple data assimilation methods.

408

## 409 **Acknowledgments**

410 This study was supported by the Excellent Young Scientist Foundation of NSFC (51422907) and the





411 Open Foundation of State Key Laboratory of Water Resources and Hydropower Engineering Science in  
412 Wuhan University (2015SWG01). The authors would like to thank the editor and the anonymous  
413 reviewers for their comments that helped to improve the quality of the paper.

414

## 415 **References**

- 416 Abaza, M., Anctil, F., Fortin, V., and Turcotte, R.: Sequential streamflow assimilation for short-term  
417 hydrological ensemble forecasting, *J. Hydrol.*, 519, 2692-2706, doi:10.1016/j.jhydrol.2014.08.038,  
418 2014.
- 419 Allen, R. G., Pereira, L. S., Raes, D., and Smith, M.: Crop Evapotranspiration-Guidelines for  
420 Computing Crop Water Requirements-FAO Irrigation and Drainage Paper 56, Food and Agriculture  
421 Organization of the United Nations, Rome, 1998.
- 422 Andréassian, V., Parent, E., and Michel, C.: A distribution-free test to detect gradual changes in  
423 watershed behavior, *Water Resour. Res.*, 39, 1252, doi:10.1029/2003WR002081, 2003.
- 424 Brigode, P., Oudin, L., and Perrin, C.: Hydrological model parameter instability: A source of  
425 additional uncertainty in estimating the hydrological impacts of climate change?, *J. Hydrol.*, 476,  
426 410-425, doi:10.1016/j.jhydrol.2012.11.012, 2013.
- 427 Brown, A. E., Zhang, L., McMahon, T. A., Western, A. W., and Vertessy, R. A.: A review of paired  
428 catchment studies for determining changes in water yield resulting from alterations in vegetation, *J.*  
429 *Hydrol.*, 310, 28-61, doi:10.1016/j.jhydrol.2004.12.010, 2005.
- 430 Clark, M. P., Rupp, D. E., Woods, R. A., Zheng, X., Ibbitt, R. P., Slater, A. G., Schmidt, J., and  
431 Uddstrom, M. J.: Hydrological data assimilation with the ensemble Kalman filter: Use of  
432 streamflow observations to update states in a distributed hydrological model, *Adv. Water Resour.*,  
433 31, 1309-1324, doi:10.1016/j.advwatres.2008.06.005, 2008.
- 434 Coron, L., Andréassian, V., Perrin, C., Lerat, J., Vaze, J., Bourqui, M., and Hendrickx, F.: Crash testing  
435 hydrological models in contrasted climate conditions: An experiment on 216 Australian catchments,  
436 *Water Resour. Res.*, 48, W05552, doi:10.1029/2011WR011721, 2012.
- 437 DeChant, C. M. and Moradkhani, H.: Examining the effectiveness and robustness of sequential data  
438 assimilation methods for quantification of uncertainty in hydrologic forecasting, *Water Resour. Res.*,  
439 48, W04518, doi:10.1029/2011WR011011, 2012.
- 440 DeChant, C. M. and Moradkhani, H.: Toward a reliable prediction of seasonal forecast uncertainty:  
441 Addressing model and initial condition uncertainty with ensemble data assimilation and sequential



- 442 Bayesian combination, *J. Hydrol.*, doi:10.1016/j.jhydrol.2014.05.045, 2014.
- 443 Delijani, E. B., Pishvaie, M. R., and Boojarjomehry, R. B.: Subsurface characterization with localized  
444 ensemble Kalman filter employing adaptive thresholding, *Adv. Water Resour.*, 69, 181-196,  
445 doi:10.1016/j.advwatres.2014.04.011, 2014.
- 446 Deng, C., Liu, P., Guo, S., Wang, H., and Wang, D.: Estimation of nonfluctuating reservoir inflow  
447 from water level observations using methods based on flow continuity, *J. Hydrol.*,  
448 doi:10.1016/j.jhydrol.2015.09.037, 2015.
- 449 Deng, C., Liu, P., Liu, Y., Wu, Z. H., and Wang, D.: Integrated hydrologic and reservoir routing model  
450 for real-time water level forecasts, *J. Hydrol. Eng.*, 20(9), 05014032,  
451 doi:10.1061/(ASCE)HE.1943-5584.0001138, 2015.
- 452 Duan, Q. Y., Gupta, V. K., and Sorooshian, S.: Shuffled complex evolution approach for effective and  
453 efficient global minimization, *J. Optimiz. Theory App.*, 76, 501-521, doi:10.1007/bf00939380,  
454 1993.
- 455 Evensen, G.: The Ensemble Kalman filter: theoretical formulation and practical implementation,  
456 *Ocean Dyn.*, 53, 343-367, doi:10.1007/s10236-003-0036-9, 2003.
- 457 Guo, S., Chen, H., Zhang, H., Xiong, L., Liu, P., Pang, B., Wang, G., and Wang, Y.: A semi-distributed  
458 monthly water balance model and its application in a climate change impact study in the middle and  
459 lower Yellow River basin, *Water International*, 30, 250-260, doi:10.1080/02508060508691864,  
460 2005.
- 461 Guo, S., Wang, J., Xiong, L., Ying, A., and Li, D.: A macro-scale and semi-distributed monthly water  
462 balance model to predict climate change impacts in China, *J. Hydrol.*, 268, 1-15,  
463 doi:10.1016/S0022-1694(02)00075-6, 2002.
- 464 Han, E., Merwade, V., and Heathman, G. C.: Implementation of surface soil moisture data assimilation  
465 with watershed scale distributed hydrological model, *J. Hydrol.*, 416-417, 98-117,  
466 doi:10.1016/j.jhydrol.2011.11.039, 2012.
- 467 Jeremiah, E., Marshall, L., Sisson, S. A., and Sharma, A.: Specifying a hierarchical mixture of experts  
468 for hydrologic modeling: Gating function variable selection, *Water Resour. Res.*, 49, 2926-2939,  
469 doi:10.1002/wrcr.20150, 2013.
- 470 Kumar, S. V., Reichle, R. H., Harrison, K. W., Peters-Lidard, C. D., Yatheendradas, S., and Santanello,  
471 J. A.: A comparison of methods for a priori bias correction in soil moisture data assimilation, *Water*  
472 *Resour. Res.*, 48, W03515, doi:10.1029/2010WR010261, 2012.
- 473 Leisenring, M. and Moradkhani, H.: Analyzing the uncertainty of suspended sediment load prediction  
474 using sequential data assimilation, *J. Hydrol.*, 468-469, 268-282, doi:10.1016/j.jhydrol.2012.08.049,  
475 2012.
- 476 Li, S., Xiong, L., Dong, L., and Zhang, J.: Effects of the Three Gorges Reservoir on the hydrological  
477 droughts at the downstream Yichang station during 2003–2011, *Hydrol. Processes* 27, 3981-3993,



- 478 doi:10.1002/hyp.9541, 2013.
- 479 Li, X.-N., Xie, P., Li, B.-B., and Zhang, B.: A probability calculation method for different grade  
480 drought event under changing environment-Taking Wuding River basin as an example, Shuili  
481 Xuebao/Journal of Hydraulic Engineering, 45, 585-594, doi:10.13243/j.cnki.slxh.2014.05.010,  
482 2014 (in Chinese).
- 483 Li, Z., Liu, P., Deng, C., Guo, S., He, P., and Wang, C.: Evaluation of the estimation of distribution  
484 algorithm to calibrate a computationally intensive hydrologic model, J. Hydrol. Eng.,  
485 doi:10.1061/(ASCE)HE.1943-5584.0001350, 2015.
- 486 Liu, Y. and Gupta, H. V.: Uncertainty in hydrologic modeling: Toward an integrated data assimilation  
487 framework, Water Resour. Res., 43(7), 1-18, doi:10.1029/2006WR005756, 2007.
- 488 Li, Y., Ryu, D., Western, A. W., and Wang, Q. J.: Assimilation of stream discharge for flood  
489 forecasting: The benefits of accounting for routing time lags, Water Resour. Res., 49, 1887-1900,  
490 doi:10.1002/wrcr.20169, 2013.
- 491 Lü, H. S., Hou, T., Horton, R., Zhu, Y. H., Chen, X., Jia, Y. W., Wang, W., and Fu, X. L.: The  
492 streamflow estimation using the Xinanjiang rainfall runoff model and dual state-parameter  
493 estimation method, J. Hydrol., 480, 102-114, doi:10.1016/j.jhydrol.2012.12.011, 2013.
- 494 Merz, R., Parajka, J., and Blöschl, G.: Time stability of catchment model parameters: Implications for  
495 climate impact analyses, Water Resour. Res., 47, W02531, doi:10.1029/2010WR009505, 2011.
- 496 Moradkhani, H., Sorooshian, S., Gupta, H. V., and Houser, P. R.: Dual state-parameter estimation of  
497 hydrological models using ensemble Kalman filter, Adv. Water Resour., 28, 135-147,  
498 doi:10.1016/j.advwatres.2004.09.002, 2005.
- 499 Nash, J. E. and Sutcliffe, J. V.: River flow forecasting through conceptual models part I: A discussion  
500 of principles, J. Hydrol., 10, 282-290, doi:10.1016/0022-1694(70)90255-6, 1970.
- 501 Nie, S., Zhu, J., and Luo, Y.: Simultaneous estimation of land surface scheme states and parameters  
502 using the ensemble Kalman filter: identical twin experiments, Hydrol. Earth Syst. Sci., 15,  
503 2437-2457, doi:10.5194/hess-15-2437-2011, 2011.
- 504 Paik, K., Kim, J. H., Kim, H. S., and Lee, D. R.: A conceptual rainfall-runoff model considering  
505 seasonal variation, Hydrol. Processes 19, 3837-3850, doi:10.1002/hyp.5984, 2005.
- 506 Panzeri, M., Riva, M., Guadagnini, A., and Neuman, S. P.: Data assimilation and parameter estimation  
507 via ensemble Kalman filter coupled with stochastic moment equations of transient groundwater  
508 flow, Water Resour. Res., 49, 1334-1344, doi:10.1002/wrcr.20113, 2013.
- 509 Patil, S. D. and Stieglitz, M.: Comparing spatial and temporal transferability of hydrological model  
510 parameters, J. Hydrol., 525, 409-417, doi:10.1016/j.jhydrol.2015.04.003, 2015.
- 511 Pauwels, V. R. N. and Lannoy, G. J. M. D.: Improvement of Modeled Soil Wetness Conditions and  
512 Turbulent Fluxes through the Assimilation of Observed Discharge, J. Hydrometeorol., 7, 458-477,  
513 doi:doi:10.1175/JHM490.1, 2006.



- 514 Peel, M. C. and Bloschl, G.: Hydrological modelling in a changing world, *Prog. Phys. Geogr.*, 35(2),  
515 249-261, doi:10.1177/0309133311402550, 2011.
- 516 Samuel, J., Coulibaly, P., Dumedah, G., and Moradkhani, H.: Assessing model state and forecasts  
517 variation in hydrologic data assimilation, *J. Hydrol.*, 513, 127-141,  
518 doi:10.1016/j.jhydrol.2014.03.048, 2014.
- 519 Seiller, G., Anctil, F., and Perrin, C.: Multimodel evaluation of twenty lumped hydrological models  
520 under contrasted climate conditions, *Hydrol. Earth Syst. Sci.*, 16, 1171-1189,  
521 doi:10.5194/hess-16-1171-2012, 2012.
- 522 Shi, Y., Davis, K. J., Zhang, F., Duffy, C. J., and Yu, X.: Parameter estimation of a physically based  
523 land surface hydrologic model using the ensemble Kalman filter: A synthetic experiment, *Water*  
524 *Resour. Res.*, 50, 706-724, doi:10.1002/2013WR014070, 2014.
- 525 Su, T., Feng, T., and Feng, G.: Evaporation variability under climate warming in five reanalyses and its  
526 association with pan evaporation over China, *Journal of Geophysical Research: Atmospheres*, 120,  
527 8080-8098, doi:10.1002/2014JD023040, 2015.
- 528 Tamura, H., Bacopoulos, P., Wang, D., Hagen, S. C., and Kubatko, E. J.: State estimation of tidal  
529 hydrodynamics using ensemble Kalman filter, *Adv. Water Resour.*, 63, 45-56,  
530 doi:10.1016/j.advwatres.2013.11.002, 2014.
- 531 Thirel, G., Andréassian, V., Perrin, C., Audouy, J. N., Berthet, L., Edwards, P., Folton, N., Furusho, C.,  
532 Kuentz, A., Lerat, J., Lindström, G., Martin, E., Mathevet, T., Merz, R., Parajka, J., Ruelland, D.,  
533 and Vaze, J.: Hydrology under change: an evaluation protocol to investigate how hydrological  
534 models deal with changing catchments, *Hydrol. Sci. J.*, 60, 1184-1199,  
535 doi:10.1080/02626667.2014.967248, 2015.
- 536 Vrugt, J. A., ter Braak, C. J. F., Diks, C. G. H., and Schoups, G.: Hydrologic data assimilation using  
537 particle Markov chain Monte Carlo simulation: Theory, concepts and applications, *Adv. Water*  
538 *Resour.*, 51, 457-478, doi:10.1016/j.advwatres.2012.04.002, 2013.
- 539 Wang, D., Chen, Y., and Cai, X.: State and parameter estimation of hydrologic models using the  
540 constrained ensemble Kalman filter, *Water Resour. Res.*, 45, W11416, doi:10.1029/2008WR007401,  
541 2009.
- 542 Wang, G. and Fan, Z.: A study of water and sediment changes in the Yellow River, Publishing House  
543 of Yellow River Water Conservancy, Zhengzhou, 2003 (in Chinese).
- 544 Weerts, A. H. and El Serafy, G. Y. H.: Particle filtering and ensemble Kalman filtering for state  
545 updating with hydrological conceptual rainfall-runoff models, *Water Resour. Res.*, 42, 1-17,  
546 doi:10.1029/2005WR004093, 2006.
- 547 Westra, S., Thyer, M., Leonard, M., Kavetski, D., and Lambert, M.: A strategy for diagnosing and  
548 interpreting hydrological model nonstationarity, *Water Resour. Res.*, 50, 5090-5113,  
549 doi:10.1002/2013WR014719, 2014.



- 550 Xie, X., Meng, S., Liang, S., and Yao, Y.: Improving streamflow predictions at ungauged locations  
551 with real-time updating: application of an EnKF-based state-parameter estimation strategy, *Hydrol.*  
552 *Earth Syst. Sci.*, 18, 3923-3936, doi:10.5194/hess-18-3923-2014, 2014.
- 553 Xie, X. and Zhang, D.: Data assimilation for distributed hydrological catchment modeling via  
554 ensemble Kalman filter, *Adv. Water Resour.*, 33, 678-690, doi:10.1016/j.advwatres.2010.03.012,  
555 2010.
- 556 Xie, X. and Zhang, D.: A partitioned update scheme for state-parameter estimation of distributed  
557 hydrologic models based on the ensemble Kalman filter, *Water Resour. Res.*, 49, 7350-7365,  
558 doi:10.1002/2012WR012853, 2013.
- 559 Xiong, L. and Guo, S.: Appraisal of Budyko formula in calculating long-term water balance in humid  
560 watersheds of southern China, *Hydrol. Processes* 26, 1370-1378, doi:10.1002/hyp.8273, 2012.
- 561 Xiong, L. and Guo, S. L.: A two-parameter monthly water balance model and its application, *J.*  
562 *Hydrol.*, 216, 111-123, doi:10.1016/S0022-1694(98)00297-2, 1999.
- 563 Xiong, L., Yu, K.-x., and Gottschalk, L.: Estimation of the distribution of annual runoff from climatic  
564 variables using copulas, *Water Resour. Res.*, 50, 7134-7152, doi:10.1002/2013WR015159, 2014.
- 565 Xu, J.: Variation in annual runoff of the Wudinghe River as influenced by climate change and human  
566 activity, *Quat. Int.*, 244, 230-237, doi:10.1016/j.quaint.2010.09.014, 2011.
- 567 Xue, L. and Zhang, D.: A multimodel data assimilation framework via the ensemble Kalman filter,  
568 *Water Resour. Res.*, 50, 4197-4219, doi:10.1002/2013WR014525, 2014.
- 569 Yan, H., DeChant, C. M., and Moradkhani, H.: Improving soil moisture profile prediction with the  
570 particle filter-Markov chain Monte Carlo method, *IEEE Trans. Geosci. Remot. Sens.*, 53, 6134-6147,  
571 doi:10.1109/tgrs.2015.2432067, 2015.
- 572 Ye, W., Bates, B. C., Viney, N. R., Sivapalan, M., and Jakeman, A. J.: Performance of conceptual  
573 rainfall-runoff models in low-yielding ephemeral catchments, *Water Resour. Res.*, 33, 153-166,  
574 doi:10.1029/96WR02840, 1997.
- 575 Zhang, D., Liu, X. M., Liu, C. M., and Bai, P.: Responses of runoff to climatic variation and human  
576 activities in the Fenhe River, China, *Stoch. Environ. Res. Risk Assess.*, 27, 1293-1301,  
577 doi:10.1007/s00477-012-0665-y, 2013.
- 578 Zhang, H., Huang, G. H., Wang, D., and Zhang, X.: Multi-period calibration of a semi-distributed  
579 hydrological model based on hydroclimatic clustering, *Adv. Water Resour.*, 34, 1292-1303,  
580 doi:10.1016/j.advwatres.2011.06.005, 2011.
- 581



582

## 583 **Tables**

584 **Table 1.** States and parameters of the two-parameter monthly water balance model.

| Parameters and state variables |      | Description                      | Ranges and unit |
|--------------------------------|------|----------------------------------|-----------------|
| Parameter                      | $C$  | Evapotranspiration parameter     | 0.2-2.0 (-)     |
|                                | $SC$ | Catchment water storage capacity | 100-4000 (mm)   |
| State variable                 | $S$  | Soil water content               | mm              |

585



586

587

**Table 2.** Different variations of model parameters in the synthetic experiment.

| Scenario   | Description   |
|------------|---|
| Scenario 1 | <i>C</i> has a periodic variation, and <i>SC</i> has an increasing trend                          |
| Scenario 2 | <i>C</i> has a periodic variation, and <i>SC</i> has an abrupt change                             |
| Scenario 3 | <i>C</i> has a periodic variation with an increasing trend, and <i>SC</i> has an increasing trend |
| Scenario 4 | <i>C</i> has a periodic variation with an increasing trend, and <i>SC</i> has an abrupt change    |
| Scenario 5 | Both <i>C</i> and <i>SC</i> are constant  |

588



589

590

Table 3. Proportional factors of the standard deviations for precipitation ( $\gamma_P$ ) and runoff ( $\gamma_Q$ ) uncertainties.

| Type       | Low level | Medium level | High level |
|------------|-----------|--------------|------------|
| $\gamma_P$ | 0         | 0.05         | 0.10       |
| $\gamma_Q$ | 0.05      | 0.10         | 0.20       |





591

592

593

**Table 4.** Performance statistics for various changes of (a) parameter  $C$  and (b)  $SC$  estimations under different levels of uncertainty in the synthetic experiment.

| Scenario                             | Low level   |             |          | Medium level |             |          | High level  |             |          |
|--------------------------------------|-------------|-------------|----------|--------------|-------------|----------|-------------|-------------|----------|
|                                      | <i>RMSE</i> | <i>MARE</i> | <i>R</i> | <i>RMSE</i>  | <i>MARE</i> | <i>R</i> | <i>RMSE</i> | <i>MARE</i> | <i>R</i> |
| <b>(a) Parameter <math>C</math></b>  |             |             |          |              |             |          |             |             |          |
| Scenario 1                           | 0.15        | 0.21        | 0.55     | 0.16         | 0.18        | 0.68     | 0.18        | 0.11        | 0.89     |
| Scenario 2                           | 0.16        | 0.19        | 0.63     | 0.17         | 0.16        | 0.75     | 0.18        | 0.09        | 0.91     |
| Scenario 3                           | 0.12        | 0.13        | 0.64     | 0.13         | 0.11        | 0.72     | 0.14        | 0.07        | 0.91     |
| Scenario 4                           | 0.13        | 0.12        | 0.70     | 0.13         | 0.10        | 0.77     | 0.14        | 0.06        | 0.93     |
| Scenario 5                           | 0           | --          | --       | 0            | --          | --       | 0           | --          | --       |
| <b>(b) Parameter <math>SC</math></b> |             |             |          |              |             |          |             |             |          |
| Scenario 1                           | 182.87      | 0.03        | 0.99     | 187.76       | 0.05        | 0.94     | 253.35      | 0.83        | 0.83     |
| Scenario 2                           | 158.30      | 0.04        | 0.96     | 167.47       | 0.07        | 0.91     | 189.59      | 0.80        | 0.80     |
| Scenario 3                           | 180.20      | 0.03        | 0.99     | 183.06       | 0.04        | 0.97     | 215.04      | 0.88        | 0.88     |
| Scenario 4                           | 156.42      | 0.03        | 0.97     | 158.50       | 0.05        | 0.93     | 170.90      | 0.86        | 0.86     |
| Scenario 5                           | 1.54        | --          | --       | 3.67         | --          | --       | 20.54       | --          | --       |

594



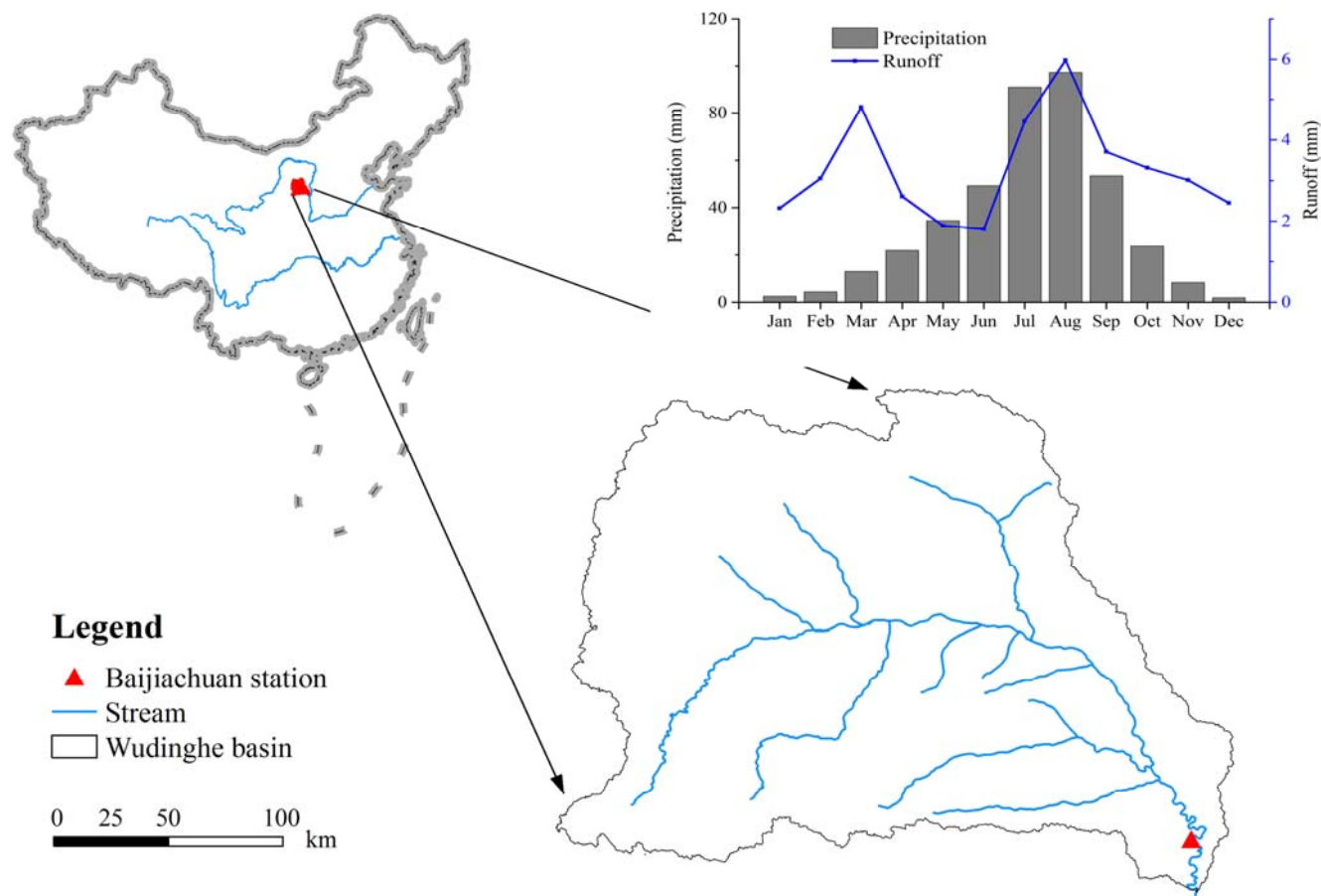
595

596 Table 5. Performance of runoff estimations for various parameter changes under different levels of uncertainty in the  
597 synthetic experiment.

| Scenario   | Low level  |           | Medium level |           | High level |           |
|------------|------------|-----------|--------------|-----------|------------|-----------|
|            | <i>NSE</i> | <i>VE</i> | <i>NSE</i>   | <i>VE</i> | <i>NSE</i> | <i>VE</i> |
| Scenario 1 | 0.999      | -0.0003   | 0.988        | -0.0046   | 0.967      | -0.0230   |
| Scenario 2 | 0.999      | 0.0001    | 0.990        | -0.0028   | 0.967      | -0.0141   |
| Scenario 3 | 0.999      | -0.0011   | 0.990        | -0.0013   | 0.974      | -0.0264   |
| Scenario 4 | 0.999      | -0.0009   | 0.992        | 0.0002    | 0.959      | -0.0147   |
| Scenario 5 | 0.999      | -0.0022   | 0.992        | -0.0077   | 0.961      | -0.0187   |



598 **Figures**

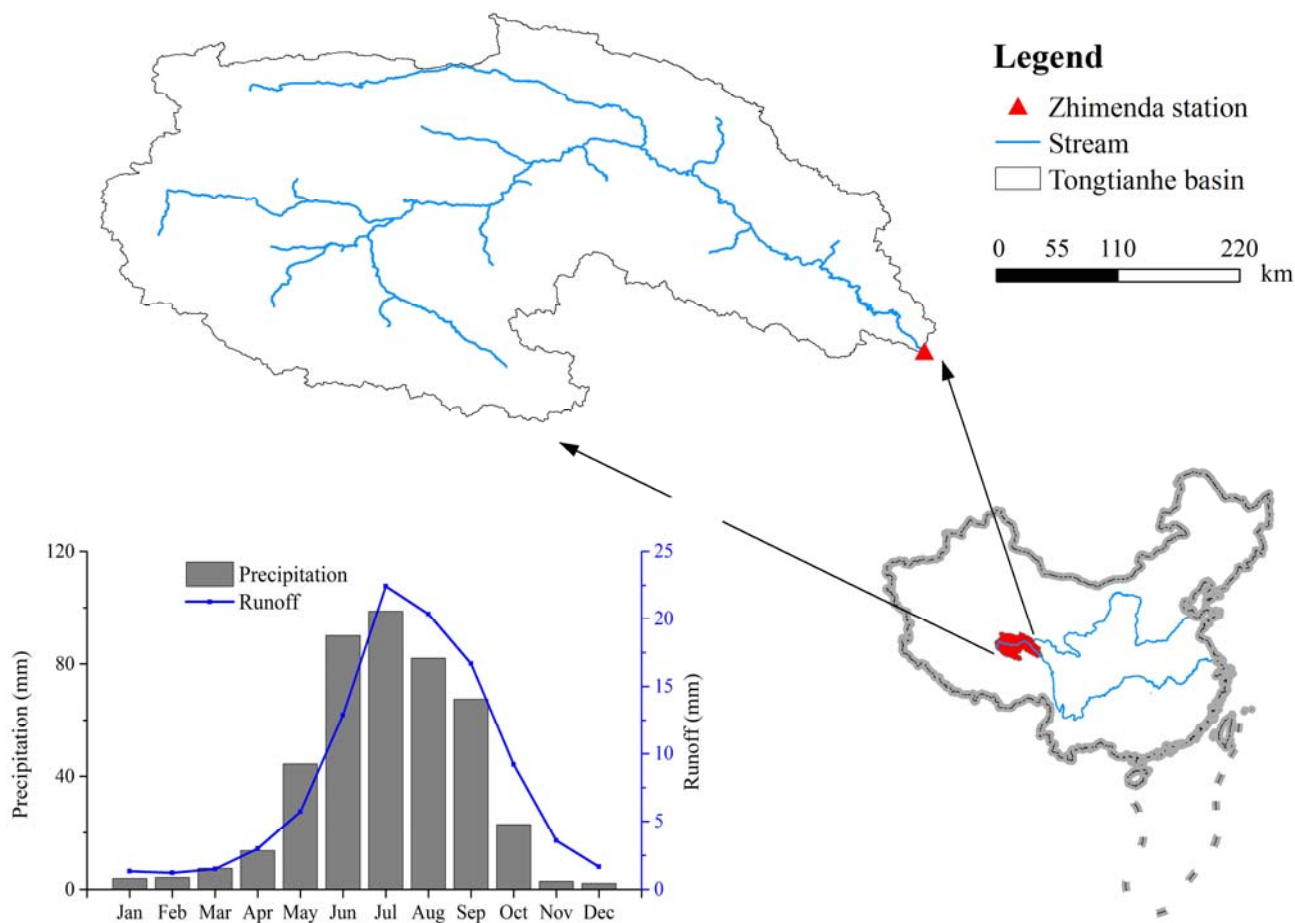


599  
600

**Figure 1.** Location and mean monthly precipitation and runoff from 1956 to 2000 of the Wudinghe basin.



601



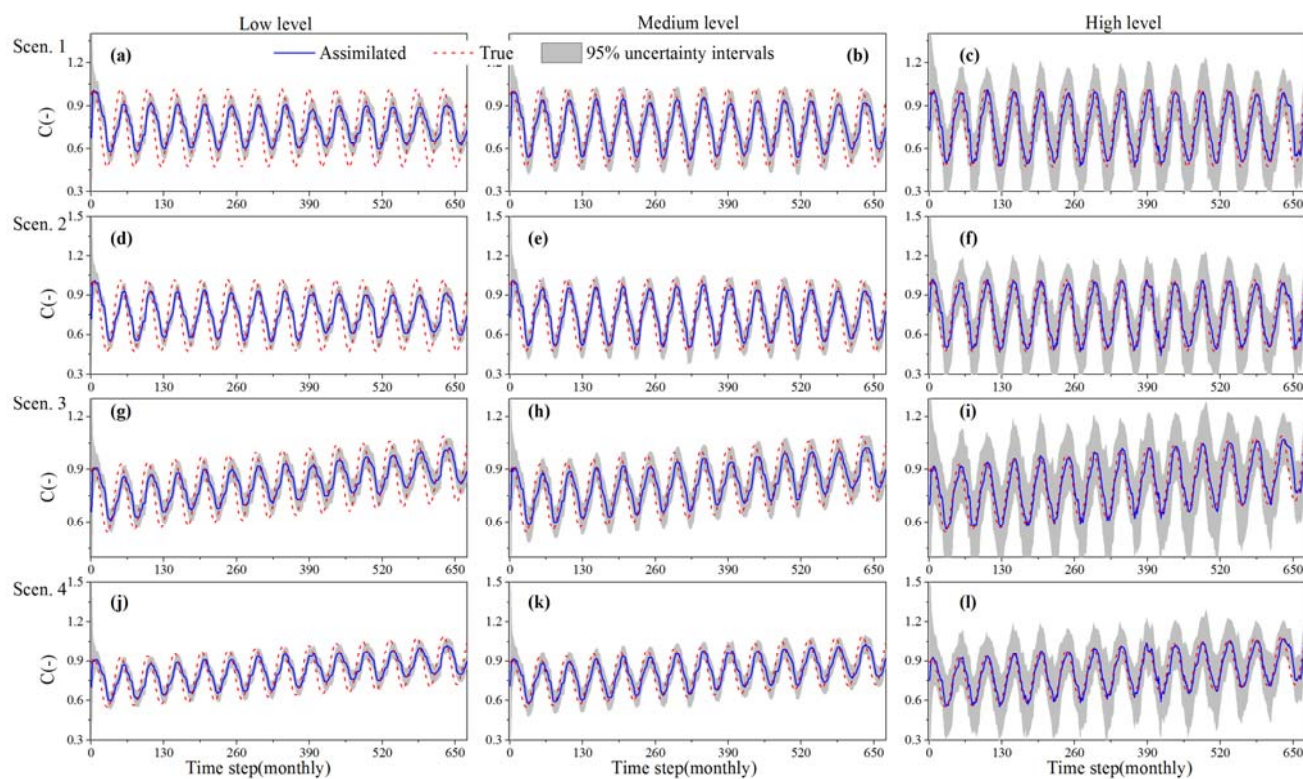
602

603

**Figure 2.** Location and mean monthly precipitation and runoff from 1980 to 2013 of the Tongtianhe basin.



604



605

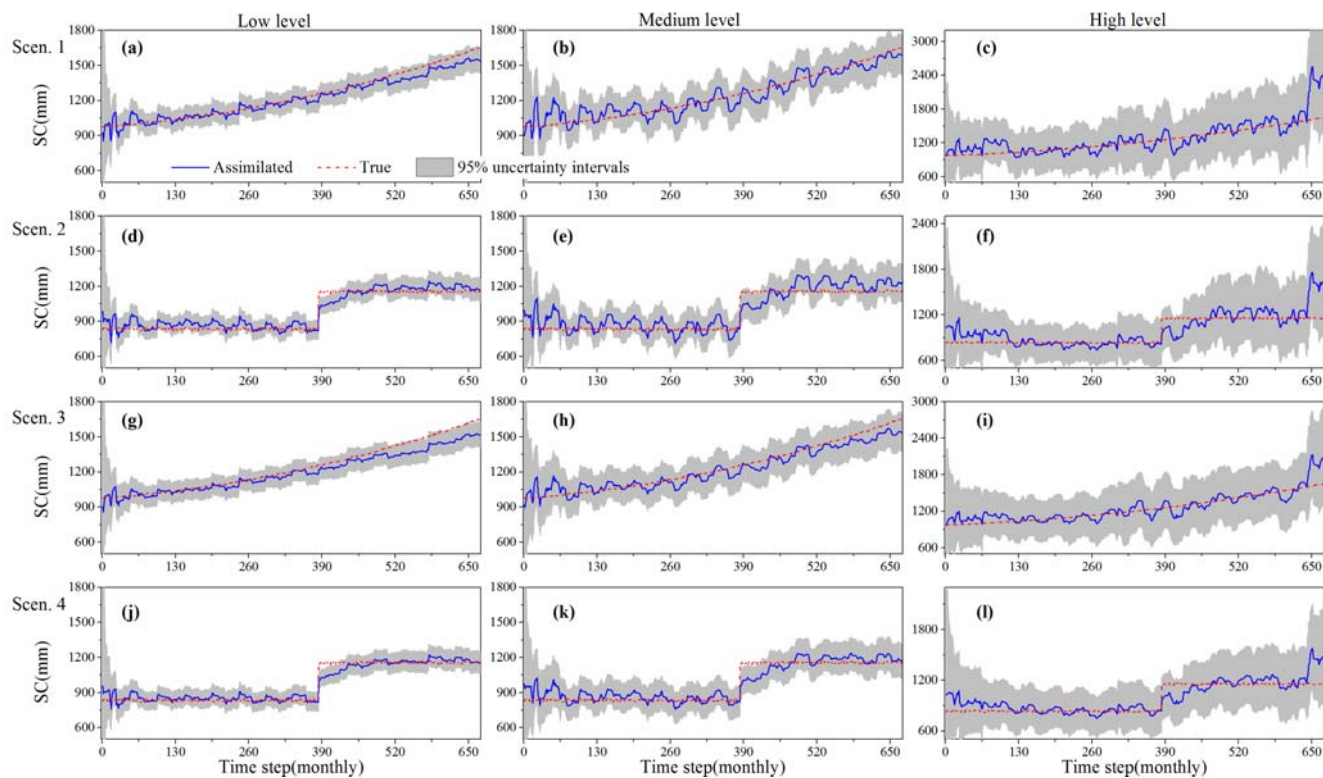
606

607

**Figure 3.** Comparison between estimated  $C$  and its true values for various parameter changes under different uncertainty levels. The grey areas represent the 95% uncertainty intervals.



608



609

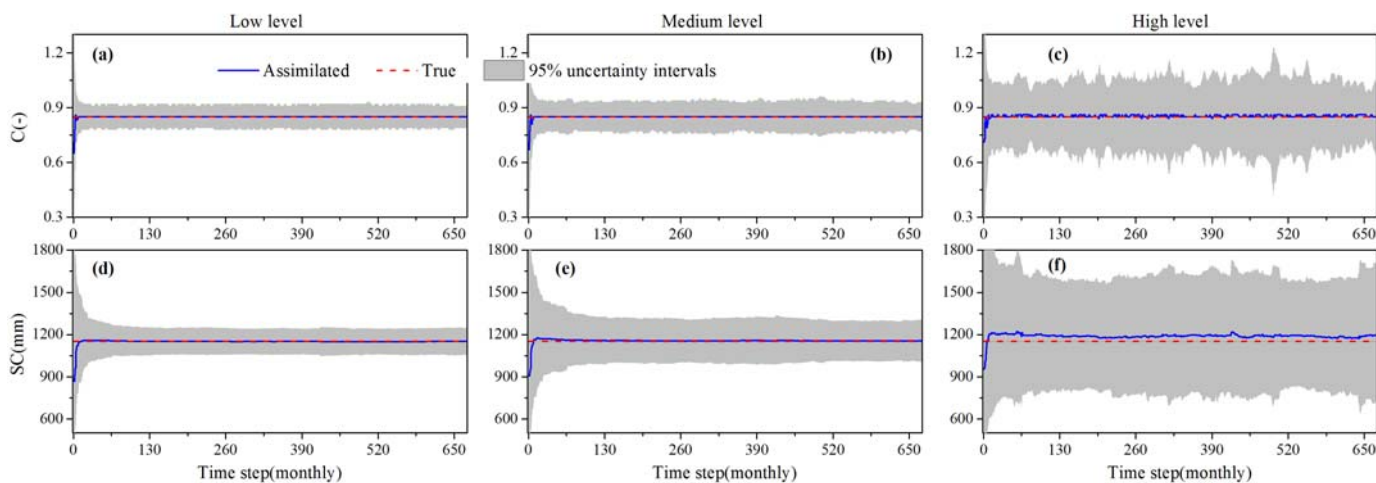
610

611

**Figure 4.** Comparison between estimated SC and its true values for various parameter changes under different uncertainty levels. The grey areas represent the 95% uncertainty intervals.



612



613

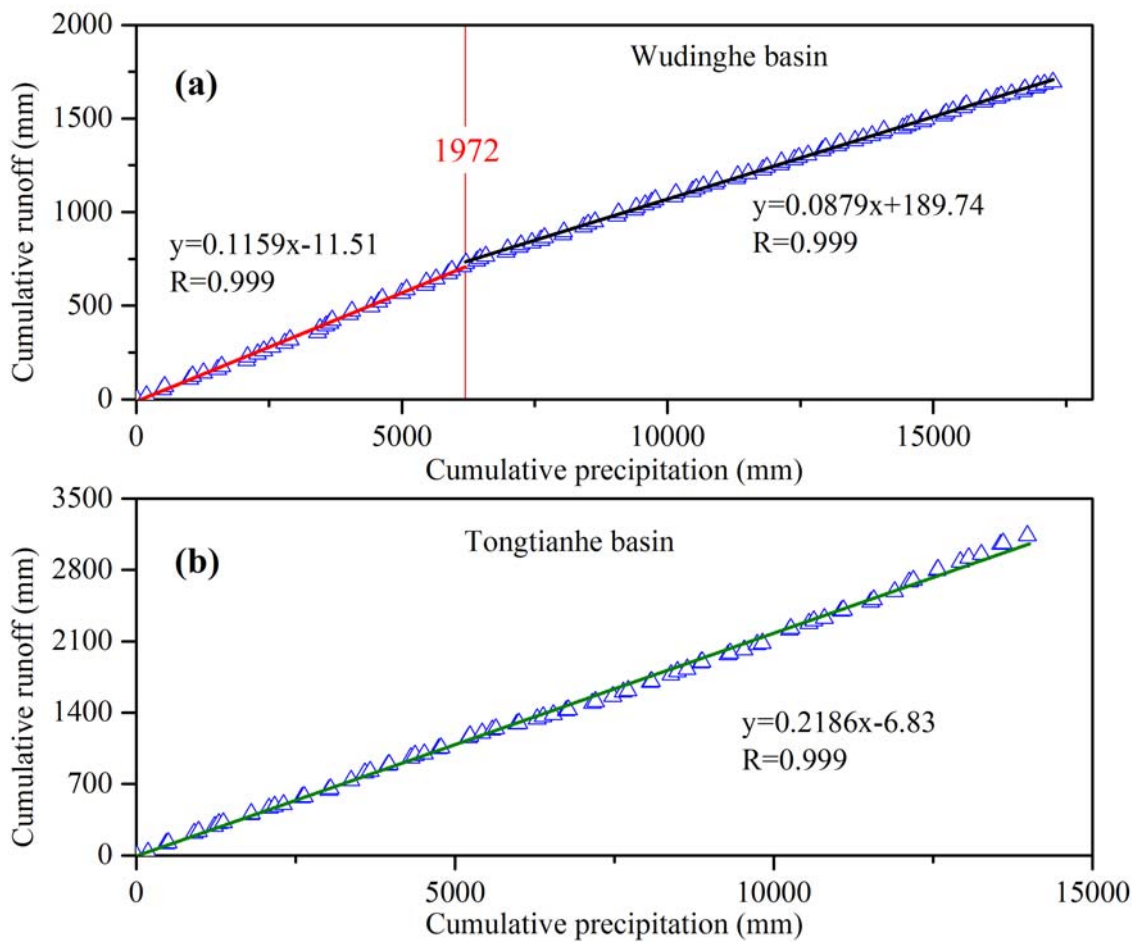
614

615

**Figure 5.** Estimations of time-invariant  $C$  and  $SC$  under different uncertainty levels. The grey areas represent the 95% uncertainty intervals.



616



617

618

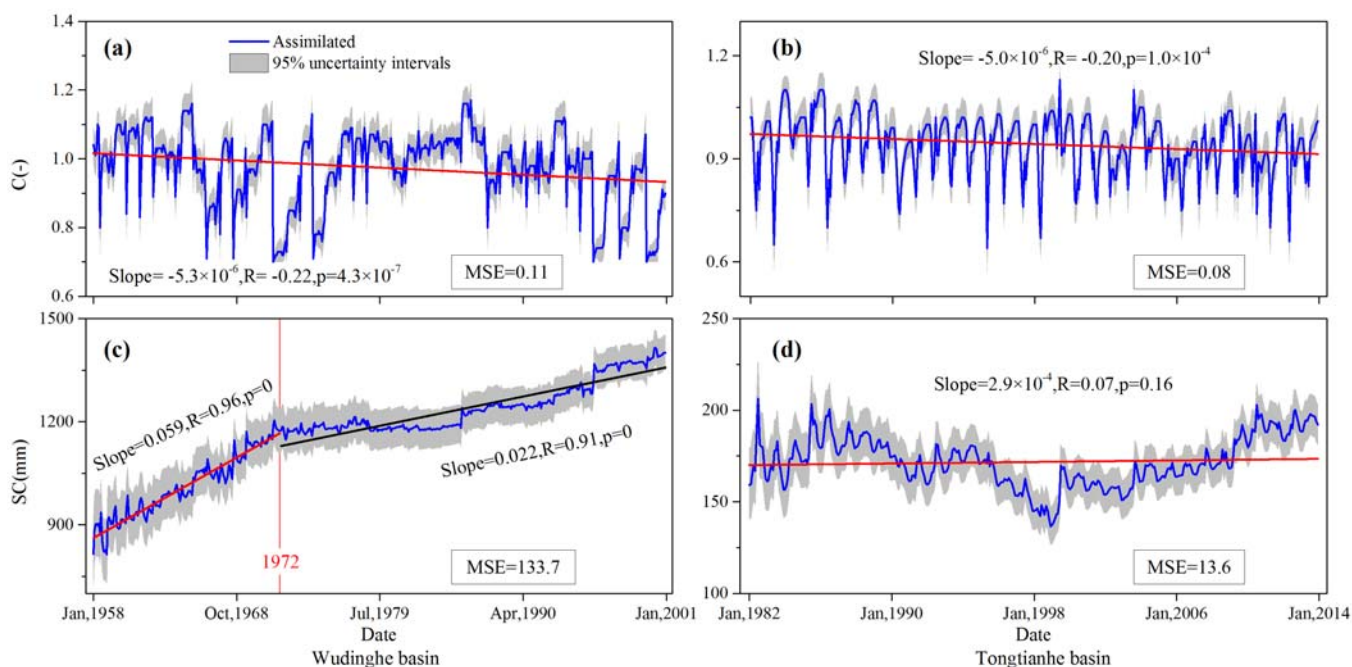
619

**Figure 6.** Double mass curve between monthly runoff and precipitation for Wudinghe basin within the period of 1958-2000 (top figure) and Tongtianhe basin within the period of 1982-2013 (bottom), respectively.





620

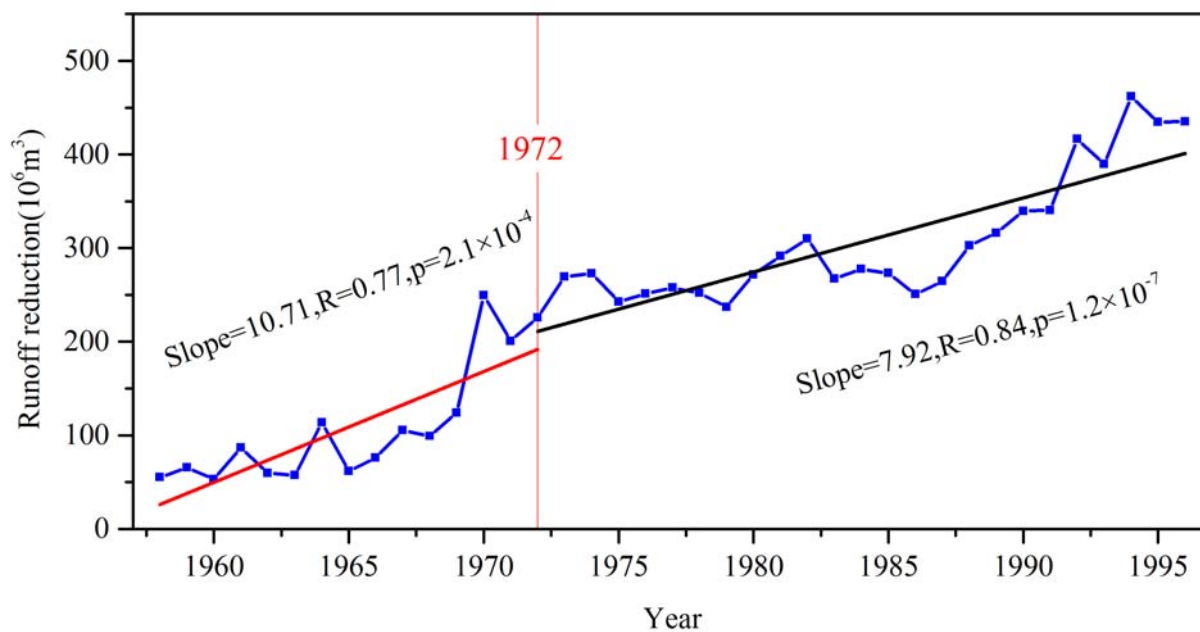


621

622 **Figure 7.** Estimated parameter values of  $C$  and  $SC$  for (1) Wudinghe basin within the period of 1958-2000, and (2)  
 623 Tongtianhe basin within the period of 1982-2013. The grey areas represent the 95% uncertainty intervals. Note that  
 624 the MSE denotes the standard deviation of the estimated parameter values.



625



626

627

628

629

**Figure 8.** Runoff reduction in Wudinghe basin caused by all the soil and water conservation measures, i.e., land terracing, tree and grass plantation, check dam and reservoir construction for the period of 1958- 1996. The data is from Wang and Fan, 2003.